Proceedings of the 24th European Young Geotechnical Engineers Conference (EYGEC), Durham, UK
Osman, A.S. & Toll, D.G. (Eds.) 2015
ISBN 978-0-9933836-01

On the stability of infinite slopes

F. Schranz[*1], W. Fellin[1]

[1] *Division of Geotechnical and Tunnel Engineering, University of Innsbruck, Austria*
[*] Corresponding Author

ABSTRACT The ultimate inclination of a cohesionless infinite slope is traditionally assumed to be equal to the friction angle of the material ($\beta = \varphi$). However, for large friction angles this assumption overestimates the stability. In this study, the maximum slope inclination is determined by numerical simple shear calculations. In the first step, an elasto-plastic material model with Mohr-Coulomb yield surface is used in order to calculate the ultimate stable inclination of a cohesionless infinite slope. Furthermore, Matsuoka-Nakai failure criterion, which provides a more appropriate yield surface for granular materials in plane strain conditions, is used for the determination of the ultimate stable inclination. Finally, the results for different dilatancy angles and different failure criteria are been compared.

1 INTRODUCTION

The model of an infinite slope is a quite simple and clear model. For these reasons it is often used in teaching to demonstrate mechanically slope stability problems (e.g. Kolymbas 2011). It can also be easily implemented in Geographical Information Systems (GIS) (Mergili & Fellin 2009; Mergili et. al. 2014).

2 CLASSIC DERIVATION

For the classic derivation of the stability of an infinite, cohesionless slope an element on the surface is cut out of the slope. The forces acting on this element are the gravity load of the soil G, reaction force on the bottom of the element Q and also reaction forces on the right side of the element E_r and E_l on the left side. The reaction force Q can be split up into a force normal to the bottom N and a force along the bottom face T (cf. Figure 1).

Due to interchangeability of elements in the infinite slope, the reaction forces E_l and E_r must have the same value, but the opposite directions. For the analysis only the gravity load G and the reaction force Q need to be considered.

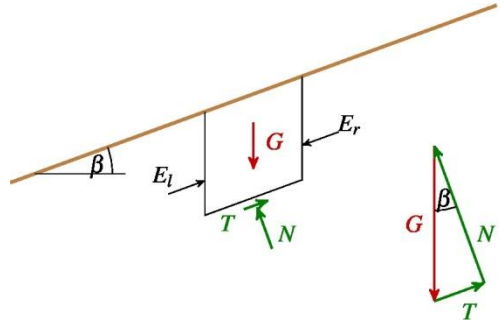

Figure 1. Element of the infinite slope with acting forces and vector sum of forces.

The vector sum of forces is also shown in Figure 1. The relation between T and N is given by the Coulomb friction model with φ as friction angle of the material in an ultimate state

$$T = N \tan\varphi \ . \qquad (1)$$

As can be seen from Figure 1, the relation between T, N and G is

$$T = G \sin\beta \text{ and } N = G \cos\beta \ . \qquad (2)$$

The forces in equation (1) can be substituted by the expressions in (2). After the elimination of G the following expression is obtained

$$\sin\beta = \cos\beta \tan\varphi, \qquad (3)$$

which can be simplified to

$$\tan\beta = \tan\varphi \ . \qquad (4)$$

This means the maximum possible inclination of a slope is equal to the friction angle of the material. However, the here shown derivation is just correct for a material with an associated flow rule (Goldscheider 2013). An associated flow rule means that the dilatancy angle ψ is equal to the friction angle φ. The dilatancy angle ψ is defined as

$$\sin\psi = \frac{\dot{\varepsilon}_v^p}{\dot{\gamma}^p} \ . \qquad (5)$$

Here $\dot{\varepsilon}_v^p$ stands for the change of the plastic volumetric strain and $\dot{\gamma}^p$ stands for the change of the plastic shear strain. The assumption $\psi = \varphi$ does not hold for granular soils. For example, Hostun Sand shows dilatancy angles ψ at the peak of triaxial tests between $\varphi_P/3$ and $\varphi_P/4$ (Desrues et. al. 2000)

3 ELASTO-PLASTIC MOHR-COULOMB MODEL

To calculate the critical slope angle in the first step the elasto-plastic Mohr-Coulomb model was used. It was assumed, that the failure of the slope corresponds to the failure in simple shear tests. For this reason numerical simple shear calculations were performed. The boundary conditions were a constant vertical normal stress σ, free deformation in vertical direction and plane strain condition (cf. Figure 2).

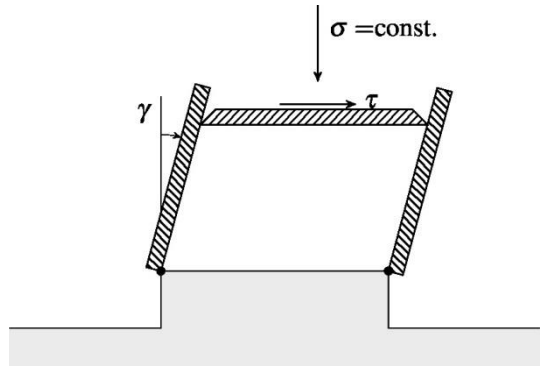

Figure 2. Schematic sketch of a Simple Shear test apparatus (c.f. Vermeer & de Borst 1984)

For the Mohr-Coulomb criterion without cohesion the yield surface f has the shape

$$f(\boldsymbol{\sigma}) = \frac{\sigma_1+\sigma_3}{2}\sin\varphi + \frac{\sigma_3-\sigma_1}{2} \ , \qquad (6)$$

where σ_1 is the minimal principal stress and σ_3 is the maximal principal stress (pressure is here defined negative). For elsto-plastic simulations also the plastic potential g has to be defined, without the integration constant g is

$$g(\boldsymbol{\sigma}) = \frac{\sigma_1+\sigma_3}{2}\sin\psi + \frac{\sigma_3-\sigma_1}{2} \ . \qquad (7)$$

As long as the yield surface f is not reached the material behaves ideal elastic

$$\boldsymbol{\sigma} = \boldsymbol{C}^e \boldsymbol{\varepsilon} \ , \qquad (8)$$

with $\boldsymbol{\varepsilon}$ being the strain and $\boldsymbol{C}^e$ the elastic material tensor. As soon as the yield surface is reached the elastic material tensor in equation (8) has to be replaced by the elasto-plastic material tensor $\boldsymbol{C}^{ep}$. The elasto-plastic material tensor is calculated with the derivation of the plastic potential with respect to stress $\boldsymbol{m}$ and the derivation of the yield surface with respect to stress $\boldsymbol{n}$

$$\boldsymbol{C}^{ep} = \boldsymbol{C}^e - \frac{\boldsymbol{m}\boldsymbol{C}^e\boldsymbol{C}^e\boldsymbol{n}^T}{\boldsymbol{m}^T\boldsymbol{C}^e\boldsymbol{n}} \ . \qquad (9)$$

A geostatic stress state was applied at the start of the computation. The shear strain increased until the changes of shear stress vanished. Figure 3 shows the evolution of the shear stress τ over the shear strain γ for the dilatancy angles $\psi = 0$, $\varphi/3$ and φ. It can be seen, that the yield surface is reached at a shear strain

γ = 0,05 % (red circle). After that the shear stress still increases for all dilatancy angles. As expected the elasto-plastic growth of the shear stress, for the higher dilatancy angles, is larger than for the smaller ones.

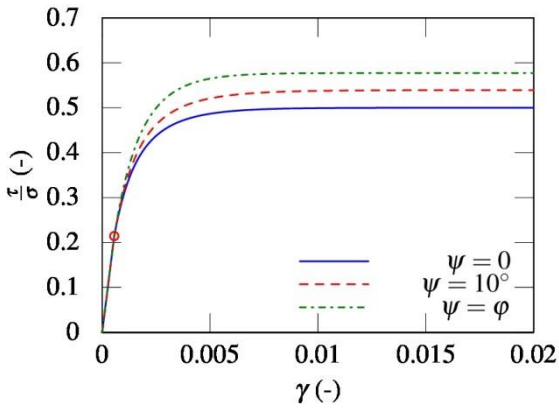

Figure 3. Shear stress as function of shear strain in a drained simple shear for different dilatancy angles (Material parameters: E = 20 MPa, ν = 0.3, φ = 30°).

The maximum inclination of the slope is given by the equation

$$\tan\beta = \frac{\tau_{max}}{\sigma} \quad . \tag{10}$$

Here τ_{max} stands for the maximum shear stress which can be achieved in the simple shear test and σ stands for the applied vertical normal stress.

From the simple shear calculation a formula can be derived which only depends on the friction and dilatancy angle of the material

$$\tan\beta = \frac{\sin\varphi \ \cos\psi}{1 - \sin\varphi \sin\psi} \quad . \tag{11}$$

This formula was first published by Teunissen and Spierenbrug (Teunissen & Spierenburg 1995). The elastic parameters (e. g. Youngs module E and Poisson's ratio ν) have no influence on the maximum inclination.

For critical states ($\psi = 0$) equation (11) shows that the maximum inclination of a slope is $\tan\beta = \sin\varphi$. This slope angle is much smaller than the angle derived from the approach with the Coulomb friction model. Furthermore the result $\beta = \varphi$ cannot be derived for any dilatancy angle ψ smaller than the friction angle φ. The result of the classical derivation can just be obtained for the associated flow ($\psi = \varphi$). In Figure 4 the required friction angles φ for given inclinations of a slope β and different reasonable dilatancy angles as like $\psi = \varphi = \beta$ are shown.

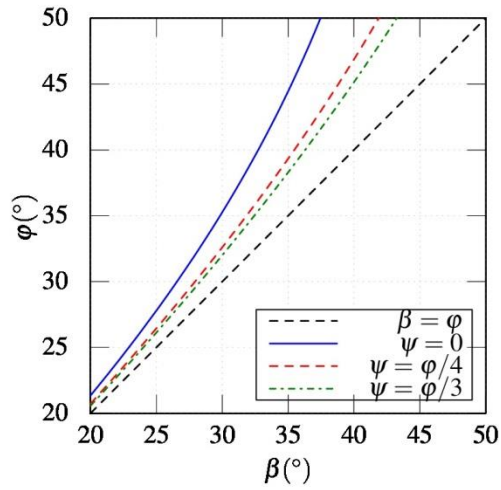

Figure 4. Maximum slope inclinations β for different dilatancy angles ψ and different friction angles φ.

It can be seen that the required friction angle is obviously larger than the slope angle for all dilatancy angles. Furthermore it can be seen, that with an increasing slope angle the necessary friction angle has to grow disproportionally for all dilatancy angles except for the case of associated flow.

However, an infinite slope is a plane strain condition and it is known that the Mohr-Coulomb criterion underestimates the strength of material for such conditions. This results from neglecting the intermediate principal stress component in the failure criterion.

4 ELASTO-PLASTIC MATSUOKA-NAKAI MODEL (MN)

For soils in plane strain conditions the Matsuoka-Nakai criterion (Matsuoka & Nakai 1974) is more appropriate than the Mohr-Coulomb criterion. In this failure criterion the intermediate principal stress has also an influence on failure

$$f(\boldsymbol{\sigma}) = I_1 I_2 - I_3 k_{MN}\,, \tag{12}$$

where I_1, I_2 and I_3 are the first, second and third invariants of stress tensor, respectively k_{MN} is a material parameter depending on the friction angle φ

$$k_{MN} = \frac{9 - \sin^2\varphi}{1 - \sin^2\varphi}\,. \tag{13}$$

An intersection with the Matsuoka-Nakai criterion and the deviatoric plane can be seen in Figure 5. In Figure 5 the Mohr-Coulomb criterion with the same friction angle is plotted as well. It can be seen, that the material strength is for both criteria the same in triaxial conditions, whereas the Matsuoka-Nakai criterion results in larger mobilized shear stresses for plane strain conditions.

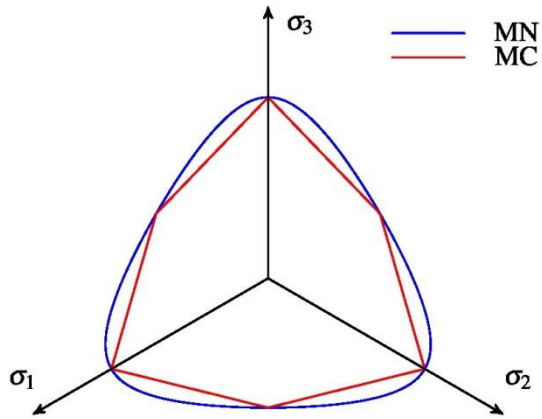

Figure 5. Intersection of Matsuoka-Nakai (MN) and Mohr-Coulomb (MC) criterion with a deviatoric plane for the same friction angle $\varphi = 30°$.

In the plastic potential g the friction angle φ cannot be substituted with the dilatancy angle ψ. This is due to the non-linearity of the failure criterion (c. f. Figure 6). Nevertheless this formulation can be used, because a cut with the deviatoric plane results in a similar figure (c. f. Figure 7). Hence it is necessary to determine the dilatancy angle ψ according to equation (5) with simple shear calculation. For example, for a friction angle of $\varphi = 30°$ dilatancy angle $\psi_{MN} = 20.1°$ has to be used in the plastic potential to achieve a dilatancy angle of $\psi = 0$ in simple shear calculations. For dilatancy angles in the plastic potential ψ_{MN} lower than the 20.1° the dilatancy angle ψ yields negative values.

The maximum inclination of a cohesionless slope with the Matsuoka-Nakai criterion cannot be derived as easily as for the Mohr-Coulomb criterion. Hence, the calculation with a simple shear test is the best possibility to get the maximum inclination of a slope. This calculation was conducted for different friction angles φ and different dilatancy angles ψ.

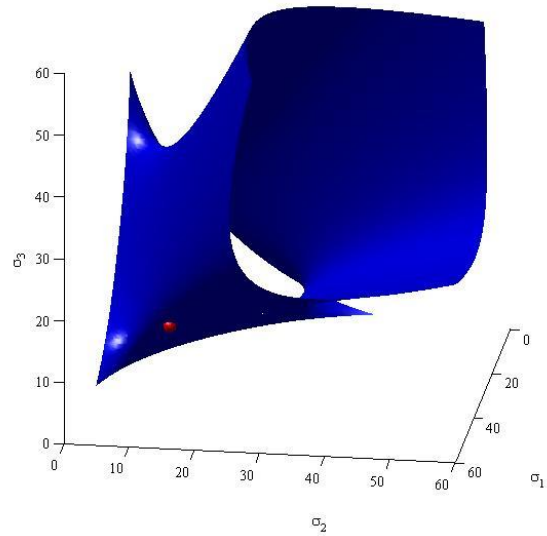

Figure 6. Matsuoka-Nakai plastic potential for $\psi \neq \varphi$ and a given stress state on the Matsuka-Nakai yield surface (red point; $\varphi = 30°$, $\psi = 0$, $g(\boldsymbol{\sigma}) = 5453$) (c. f. Schranz 2014)

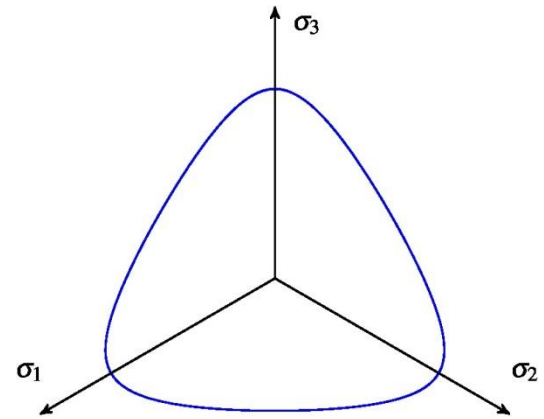

Figure 7. Intersection of Matsuoka-Nakai plastic potential ($\psi = 0$, $\psi_{MN} = 20.1°$, $g(\boldsymbol{\sigma}) = 5453$).

The results are plotted in Figure 8. It can be seen, that for friction angles φ smaller than 25° it is possible to get inclinations higher than the friction angle, even for critical states. For $\psi = \varphi/3$ it is possible to gain slope inclinations larger than the friction angle up to $\varphi = 34°$. In these cases, the classic approach is even a conservative estimation of the stability.

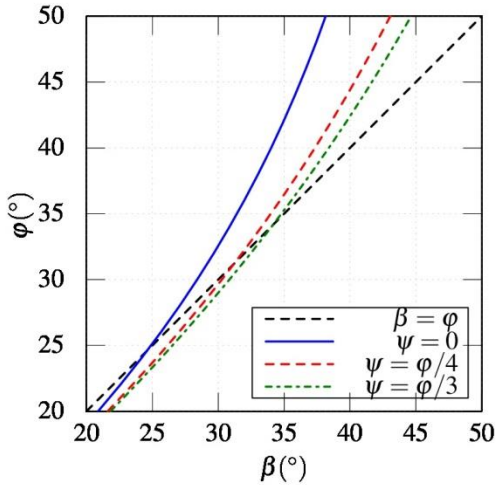

Figure 8. Maximum slope inclinations β for different dilatancy angles ψ and different friction angles φ with the Matusoka-Nakai criterion.

5 CONCLUSION

It can be shown that for the elasto-plastic material model with Mohr-Coulomb yield surface and a dilatancy angle $\psi = 0$ the maximum inclination of a cohesionless slope is

$$\tan\beta = \sin\varphi \qquad (14)$$

which is apparently smaller than the solution with a slice and the Coulomb friction model

$$\beta = \varphi. \qquad (15)$$

For dilatancy angles $\psi > 0$, the maximum inclination rises, but except for the case $\psi = \varphi$, the inclination is always smaller than φ. But this behavior is not recognized in nature, the results with the elasto-plastic material model with Mohr-Coulomb yield surface leads to very small possible slope inclinations.

The elasto-plastic material model with a Matsuoka-Nakai yield surface, which is a more suitable model for soils, yields larger possible slope inclinations than the model with Mohr-Coulomb yield surface, which is not surprising, because the yield surface in deviatoric plane has always at least the same distance to the hydrostatic axis as the Mohr-Coulomb surface. The results of the numerical simple shear tests show that for a dilatancy angle $\psi = 0$ and friction angles φ smaller than 25°, slopes with inclinations according to equation (15) are stable. For friction angles φ higher than 25° the maximum inclination is also smaller than φ. However, these friction angles are closer to the classical derivation (c. f. Figure 9). A small dilatancy angle $\psi = \varphi/3$ allows inclinations slightly larger than φ up to $\varphi = 34°$. Soils at failure at small stress levels (near the surface) typically show a significant dilatancy angle. Thus, $\beta = \varphi$ is a reasonable approximation.

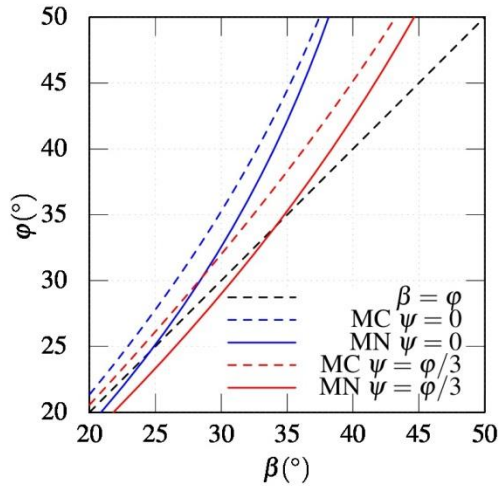

Figure 9. Maximum slope inclinations β for different dilatancy angles ψ and different friction angles φ with Mohr-Coulomb criterion (MC) and the Matsuoka-Nakai criterion (MN).

REFERENCES

Desrues, J. & Zweschper, B. & Vermeer, P.A. 2000, Database for Hostun RF Sand, *Institutsbericht 13*, Institut für Geotechnik, Universität Stuttgart.

Goldscheider, M. 2013, Gültigkeitsgrenzen des statischen Kollapstheorems der Plastomechanik für Reibungsböden, *geotechnik* **36**, 243–263.
Kolymbas, D. 2011, *Geotechnik: Bodenmechanik, Grundbau und Tunnelbau*, Springer, Berlin Heidelberg.
Matsuoka H. & Nakai T. 1974, Stress-deformation and strength characteristics of soil under three different principal stresses, *Proceedings of JSCE*, 59-74.
Mergili, M. & Fellin, W. 2009, Slope stability and geographic information systems: an advanced model versus the infinite slope stability approach, *Problems of Decrease in Natural Hazards and Risks, The International Scientifically-Practical Conference GEORISK*, 119–124.
Mergili, M. & Marchesini, I. & Rossi, M. & Guzzetti, F. & Fellin, W. 2014, Spatially distributed three-dimensional slope stability modelling in a raster GIS, *Geomorphology* **206**, 178–195.
Schranz F. 2014, Standsicherheit von unendlich langen Hängen, *Master Thesis*, Universität Innsbruck.
Teunissen, J.A.M. & Spierenburg, S.E.J. 1995, Stability of infinite slopes, *Géotechnique* **45**, No. 2, 321–323.
Vermeer, P.A. & de Borst, R. 1984, Non-associated plasticity for soils, concrete and rock, *Heron* **29**, No. 3, 1-64.